From Dislocation Junctions to Forest Hardening

R. Madec, B. Devincre, and L. P. Kubin

Laboratoire d'Etude des Microstructures, CNRS-ONERA, BP72, 92322 Châtillon Cedex, France

(Received 14 March 2002; revised manuscript received 18 June 2002; published 4 December 2002)

The mechanisms of dislocation intersection and strain hardening in fcc crystals are examined with emphasis on the process of junction formation and destruction. Large-scale 3D simulations of dislocation dynamics were performed yielding access for the first time to statistically averaged quantities. These simulations provide a parameter-free estimate of the dislocation microstructure strength and of its scaling law. It is shown that forest hardening is dominated by short-range elastic processes and is insensitive to the detail of the dislocation core structure.

DOI: 10.1103/PhysRevLett.89.255508 PACS numbers: 61.72.Lk, 62.20.Fe, 82.20.Wt

The more a crystal is deformed plastically, the larger is the stress needed to further deform it. This property, which ensures the stability of plastic flow, is called strain hardening. Its physical origin is understood in terms of dislocations, the linear defects that carry plastic flow in crystals. When two attractive dislocations gliding in different slip planes cross each other, they can reduce their total energy by reacting to form a third dislocation segment called a junction. This junction lies at the intersection of the two dislocation slip planes. It is usually not mobile and therefore represents a barrier to further dislocation motion, until the local stress is raised to a critical value such that the junction is destroyed and dislocation crossing occurs. During plastic deformation, the dislocation density increases and, as a result, the number of such events continuously increases, thus leading to strain hardening through a mechanism called forest hardening.

The objective of the present study is to establish a rigorous connection between the individual configurations of dislocation intersections and their macroscopic average strength in fcc crystals and therefore to improve the physical content of current models for strain hardening. For this purpose, use is made of a mesoscale simulation of dislocation dynamics (DD). The elementary configurations of two intersecting dislocations have been systematically studied in order to check that their individual contributions to hardening are properly accounted for in the present numerical model. Large-scale 3D simulations of forest hardening in fcc crystals are then presented, leading for the first time to a parameter-free computation of the relation between flow stress and dislocation density. The obtained scaling relation is compared to experimental data and its consequences are discussed.

The calculation of the energy of isolated junction configurations is a very complex problem [1]. In early studies it was performed using elasticity theory with strong simplifications [2,3]. More recently, a few junction configurations have been studied more precisely by atomistic [4,5] and mesoscopic simulations [6,7]. It was confirmed that the contribution of the dislocation core regions to junction stability is negligible compared to the elastic contribution from regions outside the core. For instance, it was shown that the perfect Lomer lock and the Lomer-Cottrell lock, where the core energy is reduced by dissociation and reaction of partial dislocations, have practically the same critical stress for destruction [8].

Within the forest model [2], the critical resolved stress τ to destroy a junction and remobilize the dislocation lines is proportional to $\mu b/l$, where μ is the shear modulus, b is the modulus of the Burgers vector of the mobile dislocations, and l is the distance between the intersecting obstacles along the dislocation line. The average value of this distance scales as $1/\sqrt{\rho_f}$, where ρ_f is the density of forest obstacles. This leads to a well-known relationship:

$$\tau/\mu = \alpha b\sqrt{\rho_f}, \tag{1}$$

where the constant α is an average value of the junctions strength over all existing configurations.

A major difficulty arises when performing this average, because of the wide spectrum of possible dislocation reactions [3]. Nevertheless, Eq. (1) is commonly verified by experiment. In fcc crystals, both theoretical [2,3] and experimental estimates [9,10] exist and they suggest $\alpha \approx 0.35 \pm 0.15$ (cf. the review [11]).

The constitutive rules of three-dimensional DD simulations have been discussed in several papers [12–14] (see also [15] for full details on the present simulation). Thus, for the present purpose, only a few relevant methodological aspects require a specific discussion. In each slip system, the continuous shapes of the dislocation lines are discretized into a finite number of segment directions: screw, edge, or mixed (i.e., making angles of $\pm\pi/3$ and $\pm 2\pi/3$ with the direction of the Burgers vector). This allows us to simplify the treatment of all junction segments, whose line directions at the intersection of two (111) glide planes are of either mixed or edge character. Only $a/2\langle 110\rangle\{111\}$ slip systems are explicitly accounted for (a is the lattice parameter). Additional Burgers vectors of perfect dislocations are obtained by linear combination. For instance, a particular junction, the Hirth lock,

is reproduced by superimposing segments with different Burgers vectors according to the reaction $a/2[\bar{1}10] + a/2[110] = a[010]$. As mentioned above, the dissociation of the dislocations is a core effect that needs not to be considered here. The same holds for the atomic jogs formed at the lines' intersection, as they induce a negligible resistance to dislocation motion [16]. The cross slip of screw dislocations is another important core mechanism that depends sensitively on the dissociation width of dislocations. As will be discussed below, cross slip does not appear, however, to significantly affect the intersection mechanisms. Thus, we focus here on the results obtained in conditions such that cross slip is deactivated in the simulations. The forest model is then investigated in a linear elastic and athermal (i.e., strain-rate independent) framework that does not involve any adjustable parameter.

The resolved effective force per unit length on a segment is the sum of the Peach-Koehler force and of a local line tension term balancing effects of the dislocation discretization [1]. The Peach-Koehler term accounts for the effect of the external loading and of the field of the embedding dislocation microstructure. The steady state dislocation velocity is governed by viscous drag on electron and phonons. It is of the form $v = \tau^{\star} b/B$, where $\tau^{\star} b$ is the effective force and $\tau^{\star}$ is the corresponding effective stress. B is a viscous drag constant ($B \approx 5 \times 10^{-5}$ Pa s in copper at room temperature). The model material investigated here is copper, with isotropic elastic constants $\mu = 42$ GPa, $\nu = 0.33$, and $a = 0.361$ nm. The present results can be extended to any other fcc crystal by appropriately modifying these three material constants.

Before going to large-scale simulations, one must verify that the properties of elementary configurations are well reproduced by the simulations. This is why the three possible types of junctions, namely, the Lomer, Hirth, and glissile junctions, have been examined in detail. We focus here on the Lomer lock, as some of its configurations have already been examined [5,7,8]. The two interacting slip systems are $a/2[10\bar{1}](111)$ and $a/2[011](11\bar{1})$. The tested configurations consist of two initially straight lines, pinned at their ends, of length $l_o = 30$ μm, which intersect at their midpoint. The lines initially make two angles ϕ_1 and ϕ_2, respectively, with the direction of the incipient junction. They are allowed to relax, in the absence of applied forces and under the influence of their interaction forces, until they reach a stable configuration. Three situations can occur. If the lines are attractive, they either zip a junction or, when junction formation is energetically unfavorable, they mutually pin each other at their intersection point. This last configuration is called a crossed state [6]. If the lines are repulsive, they move apart from each other.

Figure 1 shows a three-dimensional plot of the length of the Lomer lock as a function of the initial orientation of the interacting lines denoted by the angles ϕ_1 and ϕ_2.

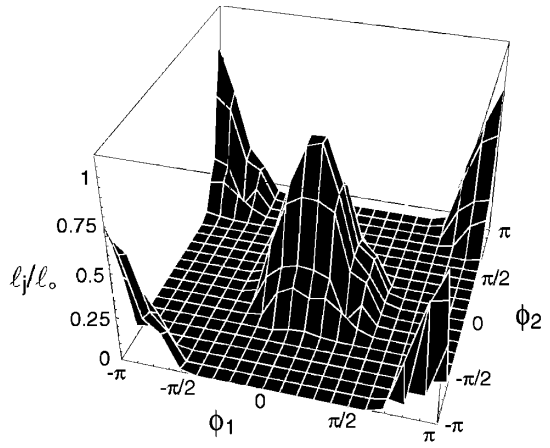

FIG. 1. Three-dimensional plot of the reduced length of the Lomer locks l_j/l_o obtained at the intersection of the two slip systems $a/2[10\bar{1}](111)$ and $a/2[011](11\bar{1})$. ϕ_1 and ϕ_2 are the initial directions of the lines with respect to the intersection of the two slip planes. Each node corresponds to a simulation result. The domain of junction formation consists of a periodic array of closed domains, with maximum junction length ($l_j/l_o = 1$) when the attractive lines are parallel. The regions where $l_j = 0$ correspond to either repulsive interactions or crossed states.

Junction formation is obtained in a periodic array of closed domains. Outside these domains, one finds another attractive region with crossed states and a region of repulsive states. The boundaries between these different types of final configurations were calculated using simplified elastic models, similar to those used in previous studies [2,3,6]. These calculations are not detailed here for the sake of brevity.

As illustrated by Fig. 1, the strength of junctions, which is inversely proportional to their length and to the lengths of the initial dislocations, critically depends on the angles ϕ_1 and ϕ_2. For the Lomer lock, it was verified that the simulated junction lengths and critical destruction stresses are the same as those previously found by other authors in the particular case $\phi_1 = \phi_2$ [5,7]. Even with the simplified geometry used here, averaging the junction strength for all values of the angles (ϕ_1, ϕ_2) involves many uncertainties. Indeed, under stress, the weakest junctions are destroyed in such a way as to provide the crystal with a sufficient density of mobile dislocations [17]. The remaining junctions have a spectrum of strengths and each strength has its own probability of occurrence. This is why only large-scale simulations can effectively integrate the contributions to the flow stress resulting from all the possible configurations of intersecting dislocations.

Large-scale simulations were carried out with several initial dislocation densities, ρ_i, in the range from 10^{10} to 10^{14} m^{-2}. These densities consisted of dislocation sources distributed at random over the 12 possible slip systems of the fcc structure. After full discretization and

relaxation, an initial microstructure with a density smaller than ρ_i was obtained. A constant total strain rate was imposed along a high symmetry [001] axis. For each density, the dimension of the simulated volume, the average length of the source segments, and the strain rate were chosen according to simple scaling laws. To fix ideas, with an initial dislocation density $\rho_i = 1.5 \times 10^{11}$ m^{-2}, a simulation cell of $26.9 \times 31.6 \times 38.9$ μm^3 was used, with a strain rate $\dot{\epsilon} = 2$ s^{-1}. Following the work of Bulatov [18], periodic boundary conditions were used in order to ensure that the dislocation densities are not affected by image forces or dislocation flux unbalance at the boundaries of the simulation cell. These conditions, although extremely useful, have to be handled with care. For instance, the incommensurate dimensions of the simulated volume are intended to limit spurious spatial correlations between the active slip planes [15].

The simulations were stopped once stable plastic flow was reached after the yield stress, which corresponded to plastic strains in the range of 10^{-4}–2.0×10^{-3}. At this point of the stress-strain curve, the average distance between dislocations, $\rho_t^{-1/2}$, where ρ_t is the total dislocation density, is at least 15 times smaller than the initial source length. This ensures that plasticity is governed by forest interactions and not by dislocation multiplication, as should be the case in typical laboratory tests. Figure 2 shows a typical dislocation microstructure obtained in such conditions for an initial density of 10^{12} m^{-2}. More detail about the stress-strain curve, dislocation microstructure, and internal stresses can be found in [17]. With a [001] stress axis, four slip systems have zero Schmid factors and are inactive, whereas eight slip systems are active with the same Schmid factor. To obtain the effective density of forest dislocations in each active slip system, ρ_f, one has to subtract from ρ_t the density of the system considered and those of its two coplanar systems. In the present case, symmetry imposes $\rho_f = 3\rho_t/4$. For each simulation, the flow stress and the final dislocation densities were measured at the maximum strain reached by the simulation.

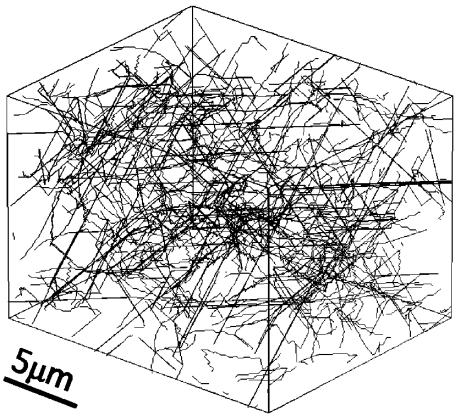

FIG. 2. The cell of the DD simulation and a dislocation microstructure at a plastic strain of 2.0×10^{-3}.

The simulation results are shown in Fig. 3. These results are subject to two causes of uncertainty. One arises from fluctuations on the simulated stress-strain curves, which are inherent to the small volumes investigated and the other from the statistical influence of the initial configurations. The resulting relative error is always within $\pm 5\%$. For comparison, we reproduce in Fig. 3 a compilation of experimental data on Cu and Ag [9] and more recent experimental results on pure Al [19].

For densities in the range of 10^{12} m^{-2}, where many measurements have been performed, the simulation yields the currently quoted value $\alpha \approx 0.35$. Considering, however, the whole range of numerical data, one can see from Fig. 3 that the average slope is not fully consistent with the square root relationship predicted by Eq. (1). In fact, α substantially decreases with increasing forest density, from about 0.5 to about 0.2. This discrepancy has already been mentioned by Basinski and Basinski [9]. Indeed, Eq. (1) makes use of a simplified form for the line tension, which omits a logarithmic term including an inner core radius ($\approx b$) and an outer cutoff radius ($\approx 1/\sqrt{\rho_f}$) taking into account self-screening due to line curvature [9,11]. Upon reintroducing this contribution, which is accounted for in the simulations, Eq. (1) becomes

$$\tau/\mu = k \ln(\rho_f^{-1/2}/b) b \sqrt{\rho_f}, \tag{2}$$

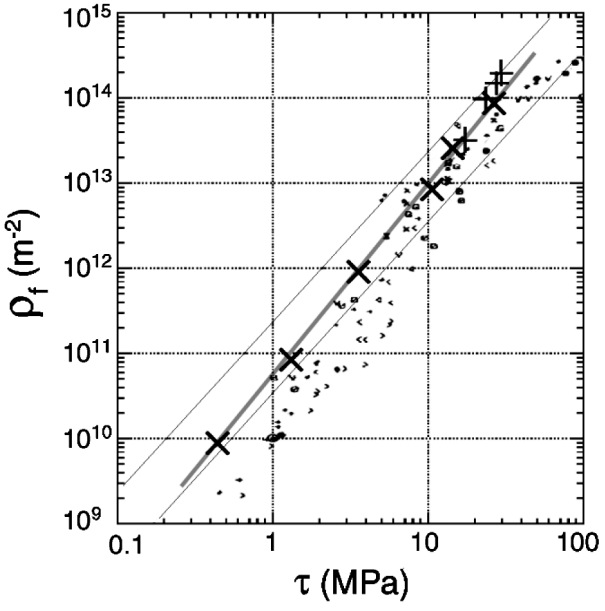

FIG. 3. Logarithmic plot of the forest dislocation density, ρ_f, vs the corresponding flow stress τ. $\times$: simulation results, regression line in grey. $+$: rescaled experimental results on aluminum after [19]. Small symbols: experimental results on Cu and Ag, after [9]. The two thin lines are plots of Eq. (1) with $\alpha = 0.2$ and 0.5.

where k is a constant that again represents the average strength of the forest. Equation (2), with $k = 0.1$, perfectly fits the present numerical data. The simulated results globally fall in the left region of the cloud of earlier data, which corresponds to the cleanest experiments. Equation (2) is also fully consistent with the more recent experimental results at high densities [10,19]. This gives confidence that no contribution to forest hardening that is accessible to experiment is missing in the simulation.

The present results apply to all pure fcc crystals, as illustrated by Fig. 3 in the cases of Cu, Al, and Ag. For instance, it was noticed long ago [9] that in all pure fcc crystals, the athermal deformation stage (stage II), which is governed by forest intersections, exhibits an almost constant strain hardening coefficient of about $\mu/250$.

In multislip conditions, such as the ones used in the present study, dislocation cross slip and dynamic recovery come into play. The scaling law of the forest mechanism [Eq. (2)] nevertheless holds all through the range of dislocation densities, stresses, and strains which has been experimentally investigated. As a matter of fact, at large stresses, Fig. 3 includes both results from poorly organized simulated microstructures and experimental data obtained in conditions where well-formed dislocations cells are necessarily present. The fact that dislocation patterning does not influence notably the value of α has puzzled many authors (see, e.g., [9,10]). Cross slip influences the dislocation density evolution and is responsible for the formation of dislocation patterns. Thus, simulations were carried out in the same conditions as above but taking cross slip into account. In agreement with expectation, heterogeneous microstructures are then formed [17], but the forest constant increases from $k = 0.1$ to $k = 0.109$ only. A tentative explanation for this paradoxical behavior was proposed by Neuhaus and Schwink [10]. Self-organized dislocation microstructures are arranged according to scaling laws such that their flow stress is almost independent of the degree of heterogeneity. It appears now that simulation methods may be of some help in clarifying this question.

Finally, one must notice that the flow stress given by Eq. (2) contains a specific signature of local line curvatures, the logarithmic term. Indeed, the Peach-Koehler forces/stresses induced on the intersecting lines by other loops do not include logarithmic terms whatever the spatial arrangement of the microstructure. Thus, the flow stress of fcc crystals deformed in the multislip condition is dominated by short-range interactions and contact reactions.

In summary, the forest mechanism has been reproduced numerically within an elastic framework that involves no adjustable parameter. The present results consistently show that no core effects appear for fcc crystals when cross slip and climb are suppressed. These results clearly show that DD simulations provide an efficient solution to the problem of averaging the extended spectrum of dislocation interactions during plastic deformation. Thus, a robust connection is established for the first time between the local properties of junction configurations and the resulting flow stress of the bulk material. In parallel, this approach allows one to examine microstructural evolutions under stress. This opens the way for novel types of studies in which, for instance, the global material hardening could be decomposed into a set of contributions stemming from pair interactions between the various slip systems.

[1] J. P. Hirth and J. Lothe, *Theory of Dislocations* (McGraw-Hill, New York, 1982).
[2] G. Saada, Acta Metall. **8**, 841 (1960).
[3] G. Schoeck and R. Frydman, Phys. Status Solidi (b) **53**, 661 (1972).
[4] V. V. Bulatov, F. F. Abraham, L. P. Kubin, B. Devincre, and S. Yip, Nature (London) **391**, 669 (1998).
[5] D. Rodney and R. Phillips, Phys. Rev. Lett. **82**, 1704 (1999).
[6] L. K. Wickham, K. W. Schwarz, and J. S. Stölken, Phys. Rev. Lett. **83**, 4574 (1999).
[7] V. B. Shenoy, R. V. Kukta, and R. Phillips, Phys. Rev. Lett. **84**, 1491 (2000).
[8] C. Shin, M. Fivel, D. Rodney, R. Phillips, V. B. Shenoy, and L. Dupuy, J. Phys. IV (France) **11**, 19 (2001).
[9] S. J. Basinski and Z. S. Basinski, *Dislocations in Solids* (North-Holland, Amsterdam, 1979), Vol. 4, pp. 261–362.
[10] R. Neuhaus and C. Schwink, Philos. Mag. A **65**, 1463 (1992).
[11] J. G. Sevillano, in *Materials Science and Technology*, edited by H. Mughrabi (VCH, Weinheim, 1993), Vol. 6, p. 19.
[12] B. Devincre, in *Computer Simulation in Materials Science: Nano/Meso/Macroscopic Space & Time Scales*, edited by H. O. Kirchner, L. P. Kubin, and V. Pontikis (Kluwer Academic Publishers, Dordrecht, Boston, 1996), pp. 309–323.
[13] H. M. Zbib, M. Rhee, and J. P. Hirth, Int. J. Mech. Sci. **40**, 113 (1998).
[14] K. W. Schwarz, J. Appl. Phys. **85**, 108 (1999).
[15] R. Madec, Ph.D. thesis, University of Orsay, 2001.
[16] J. Friedel, *Dislocations* (Pergamon Press, Oxford, 1964).
[17] R. Madec, B. Devincre, and L. P. Kubin, Scr. Metall. **47**, 689 (2002).
[18] V. V. Bulatov, M. Rhee, and W. Cai, in *Multiscale Modeling of Materials–2000*, edited by L. Kubin *et al.* (Materials Research Society, Warrendale, PA, 2001), Vol. 653, p. Z1.3.1.
[19] N. Hansen and X. Huang, Acta Mater. **46**, 1827 (1998).